Journal of Engineering Science and Technology
Vol. 8, No. 4 (2013) 457 - 471
© School of Engineering, Taylor's University

EXPERIMENTAL EVALUATION OF NUMERICAL MODELS TO REPRESENT THE STIFFNESS OF LAMINATED ROTOR CORES IN ELECTRICAL MACHINES

HIDERALDO L. V. SANTOS[1], MARCO A. LUERSEN[2,*], CARLOS A. BAVASTRI[3]

[1]WEG Electrical Equipments S.A., Jaraguá do Sul, SC, Brazil
[2]Structural Mechanics Laboratory (LaMEs), Federal University of Technology - Paraná (UTFPR), Curitiba, PR, Brazil
[3]Mechanical Engineering Department, Federal University of Paraná (UFPR), Curitiba, PR, Brazil
*Corresponding Author: luersen@utfpr.edu.br

Abstract

Usually, electrical machines have a metallic cylinder made up of a compacted stack of thin metal plates (referred as laminated core) assembled with an interference fit on the shaft. The laminated structure is required to improve the electrical performance of the machine and, besides adding inertia, also enhances the stiffness of the system. Inadequate characterization of this element may lead to errors when assessing the dynamic behavior of the rotor. The aim of this work was therefore to evaluate three beam models used to represent the laminated core of rotating electrical machines. The following finite element beam models are analysed: (i) an "equivalent diameter model", (ii) an "unbranched model" and (iii) a "branched model". To validate the numerical models, experiments are performed with nine different electrical rotors so that the first non-rotating natural frequencies and corresponding vibration modes in a free-free support condition are obtained experimentally. The models are evaluated by comparing the natural frequencies and corresponding vibration mode shapes obtained experimentally with those obtained numerically. Finally, a critical discussion of the behavior of the beam models studied is presented. The results show that for the majority of the rotors tested, the "branched model" is the most suitable

Keywords: Rotordynamics, Laminated core, Electrical machines, Natural frequencies.

Nomenclatures

CG	Center of gravity
E_{core}	Equivalent Young's modulus of the laminated core (used in model 2), GPa
H_{CO}	Height of the yoke of the rotor plate, m
Kc	Total stiffness of the sprigs used in model 3, N/m
L_{AC}	Length of the shorting rings, m
L_{CH}	Total length of the laminated core, m
L_{SHAFT}	Length of the shaft, m
M_{CH}	Mass of the laminated core, kg
M_{SHAFT}	Mass of the shaft, kg
M_T	Total mass of the core, kg
pt	Increase applied to the shaft's diameter (varies from 0 to 1)
R_E	Radius of the shaft in the core region, m

Greek Symbols

$\Delta\phi_E$	Increase in the diameter of the shaft to simulate the stiffening effect, m
ϕ_{AC}	Outer diameter of the shorting rings, m
ϕ_{CH}	Diameter of the laminated core, m
ϕ_{CO}	Diameter of the yoke of the plates in the core, m
ϕ_E	Diameter of the shaft at the core position, m
ϕ_{EQV}	Equivalent shaft diameter at the core position, m
λ_i	Eigenvalue ($\lambda_i = \omega_i^2$)
ρ_E	Mass density of the shaft's material, kg/m^3
ω_i	i-th natural frequency, rad/s

1. Introduction

In the mechanical design of an electrical machine, all the machine's functional requirements must be well defined to ensure its durability, operating reliability, performance and environmental acceptability. The majority of these requirements are inextricably linked to the vibration behavior of the machine and are usually addressed by international standards [1]. The existing body of knowledge about rotordynamics has made possible significant advances in the design of rotating systems to satisfy these standards [1-3]. Nevertheless, there is still scope for improvement of certain critical aspects. Specifically, there are few studies in the literature that address the way in which the laminated cores of electrical machines are modeled, despite the importance of this issue for the dynamics of the system. In general, it is difficult to determine how much stiffness a lamination stack imparts to the rotor when it is mounted on the shaft with an interference fit. The API 684 standard [4] states that it is a challenge to determine the amount of stiffness a lamination stack adds to the shaft and recommends, as an approximation, that the outer diameter of the shaft in the region of the stack be considered to have increased so that the additional mass is equal to the mass of the laminated core. This new "equivalent" diameter is used to take into account the increased stiffness of the shaft imparted by the lamination stack.

Kim and Kim [5] presented the results of a numerical and experimental study of the relationship between the lamination pressure used to assemble the lamination stack and the percentage increase that must be applied to the actual diameter of the shaft to take into account the stiffening effect. The authors used a 642 kg rotor consisting of just the shaft and laminate without slots for the squirrel cage bars as a test rig. The interference between the outer diameter of the shaft and the inner diameter of the lamination stack was 0.01mm. Ignoring the effect of rotation and temperature, they recommended that the shaft diameter at the core region be increased from 17% to 23% of the value of the difference between the outer and inner core diameters. Their conclusions were based on an experiment that determined the first three natural frequencies and corresponding mode shapes of the rotor in a free-free condition. The modal analysis was repeated for different lamination pressures, and the natural frequencies were obtained for each condition. The authors noticed that the natural frequencies increased with increasing lamination pressure. This increase was not directly proportional to the pressure, and for high lamination pressures the natural frequencies did not change significantly. Chen et al. [6] described a more comprehensive method for modeling the whole electrical machine. They used a parallel-beam (shaft and lamination stack) finite element model to represent a rotor with a laminated core. In this model the elements are connected node to node by springs. The properties of the lamination stack material were adjusted using experimental measurements of the natural frequencies of the rotor in a free-free condition. Garvey et al. [7] suggested modeling the laminated core as an orthotropic material by establishing a new definition of the stress-strain state that considers the flexibility between the sheets of the core. Two configurations were investigated. In the first, the elements that represent the shaft and the stack are superimposed so that their ends are connected by the same nodes, in an approach known as the "unbranched model". The second configuration - the "branched model" - uses elements in parallel connected by springs and dampers in an approach similar to that described by Chen et al. [6].

The initial objective of this work was to verify whether different geometries and/or vibration modes of squirrel-cage rotors can be represented with the same beam model using only one unknown a priori parameter value, which is determined experimentally. We evaluated the following three versions of equivalent beam models: (i) a model using an equivalent shaft diameter in the core region, referred to here as the "equivalent diameter model", (ii) a model using different finite elements to represent the laminated core and the shaft, with their ends connected by the same nodes, referred to as the "unbranched model" and (iii) a model similar to that described in (ii) but with all the ends of the shaft and laminated elements connected by springs, known, for this reason, as the "branched model". Each model is detailed in Section 2. The general objective of this work was therefore to implement the three equivalent beam models using the finite element method and carry out experiments to evaluate the behavior of the models for squirrel cage rotors with different geometries. Because of the difficulties of carrying out experiments in rotating systems, the experimental analysis was performed in non-rotating conditions. The models were evaluated by comparing the natural frequencies and corresponding vibration mode shapes obtained experimentally in a free-free support condition with those obtained by finite element analysis. It is known that the rotor rotation and the supports will change the dynamic characteristics of the systems, but this work intends to be a first step done by the authors in this research area.

2. Description of the Numerical Models

2.1. Model 01: equivalent diameter

The best-known and most widely used approach for modeling any part assembled on a shaft, including a laminated core, is to increase the diameter of the shaft in that region. The new diameter is referred to as the "equivalent diameter". The laminated core is thus considered part of the shaft, adding mass and inertia and contributing to the total stiffness of the rotor [5].

The laminated core consists of a cylinder made up of stacked sheets with a total length L_{CH}, diameter ϕ_{CH} and mass M_{CH}, the latter including the mass of the copper or aluminium bars, Fig. 1(a). The two shorting rings at both ends of the laminated core are identical and are of length L_{AC}, outer diameter ϕ_{AC} and mass M_{AC}; their center of gravity (CG) is at a distance d from the corresponding end plate of the stack.

In model 01, the shaft diameter ϕ_E at the core position is increased by $\Delta\phi_E$, Fig. 1(b). This increase in the diameter of the shaft simulates the stiffening effect of the laminated stack, in an approach similar to that described by Lalanne and Ferraris [2] to take into account the effect of discs assembled on the shaft. The new diameter in the core region is referred to as ϕ_{EQV} and is given by

$$\phi_{EQV} = \phi_E \left(1 + pt\right) \tag{1}$$

where pt is the increase applied to the diameter of the shaft and varies from 0 to 1 (corresponding to 0% and 100% of the actual diameter of the shaft, respectively). The rest of the laminated stack - the outer core diameter minus the equivalent diameter (ϕ_{CH} - ϕ_{EQV}) - is then divided into N discs whose mass and inertia are concentrated at the shaft nodes created in the stack region, while the mass and inertia values of the shorting rings are translated to the end plates of the stack, Fig. 1(b). This assembly is converted into an equivalent beam system with concentrated mass and inertia elements calculated to maintain the original mass and inertia of the whole system, Fig. 1(c).

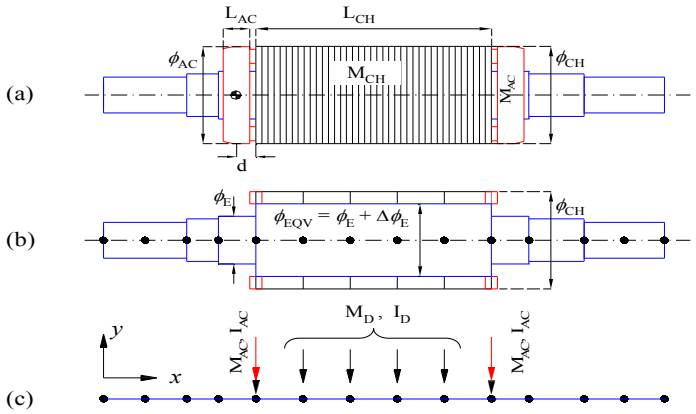

Fig. 1. Sequence of Steps Required to Represent the Laminated Core by an Equivalent Shaft Diameter: (a) Solid Model, (b) Equivalent Solid Model and Equivalent Beam Model (c).

In the model described above, the only unknown parameter or variable is *pt,* which defines the equivalent diameter in the core region. The other parameters in the model can be obtained directly from the rotor characteristics. Kim and Kim [5] found experimentally that *pt* varied from 0.28 to 0.36. They also established a second method of determining the equivalent diameter, using more information about the rotor characteristics and the following equation:

$$\phi_{EQV} = \phi_E + (\phi_{CH} - \phi_E)\, pt \tag{2}$$

Using this definition, the authors found experimentally that *pt* varied from 0.17 to 0.23 depending on the mode of vibration of the rotor. In both approaches, the value of *pt* changes according to the rotor being used and the natural vibration mode shape of the rotor.

According to the recommendation contained in [4] (API Standard, mentioned in Section 1), the increase in diameter must be such that the total mass of the laminated core M_{CH} is preserved, so that

$$\rho_E\ L_{CH}\ \frac{\pi\left(\phi_{EQV}{}^2 - \phi_E{}^2\right)}{4} = M_{CH} \tag{3}$$

where

$$\phi_{EQV} = \sqrt{\frac{4M_{CH}}{\pi\rho_E\ L_{CH}} + \phi_E{}^2} \tag{4}$$

In this case, ϕ_{EQV} is not expressed as a function of *pt*.

2.2. Model 02: unbranched model

In this approach, the laminated stack is modeled as a continuous hollow cylinder with equivalent elastic properties to simulate the effect of the stack [7]. If the cylinder is assumed to be assembled on the shaft with an interference fit, the resulting cross section will be a compound one with two materials, Fig. 2(b). To convert this system to a finite element model, in the core region we used two superimposed beam elements joined at their ends by the same node, Fig. 2(c). For both elements the Timoshenko beam model with isotropic material was used, although Garvey et al. [7] suggested a new formulation for the elements of the laminates, using an equivalent orthotropic material. In model 02 the effect of the laminated stack can be achieved by changing the Young's modulus of the laminated cylinder elements E_{core}. Using the approach described above, the only unknown parameter or model variable is E_{core}, the other model parameters being obtained directly from the rotor characteristics.

2.3. Model 03: branched model

In the branched model, the stack and shaft assembly is represented by a dual rotor system connected node-to-node by springs with a total stiffness *Kc*, Fig. 3. The laminated stack is again modeled with the same kind of beam elements used for the shaft and is represented as a hollow cylinder with the same isotropic material properties as the shaft. The lamination effect can be adjusted by varying *Kc*, the only parameter in this model.

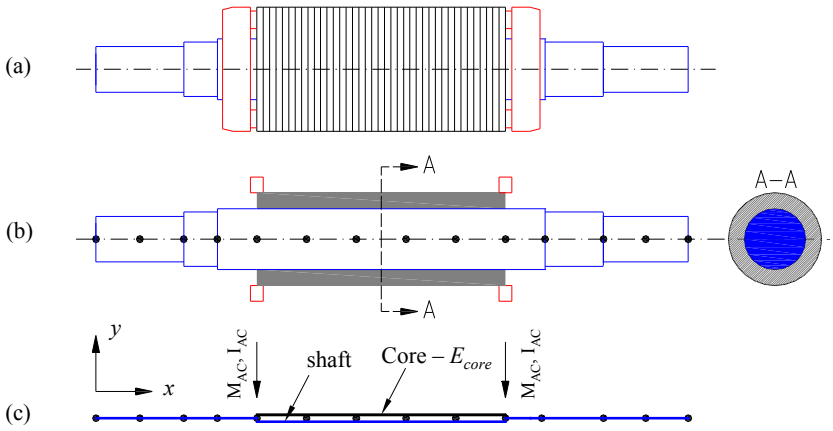

Fig. 2. Schematic Diagram of Lamination Stack Represented as a Parallel Beam (Unbranched Model).

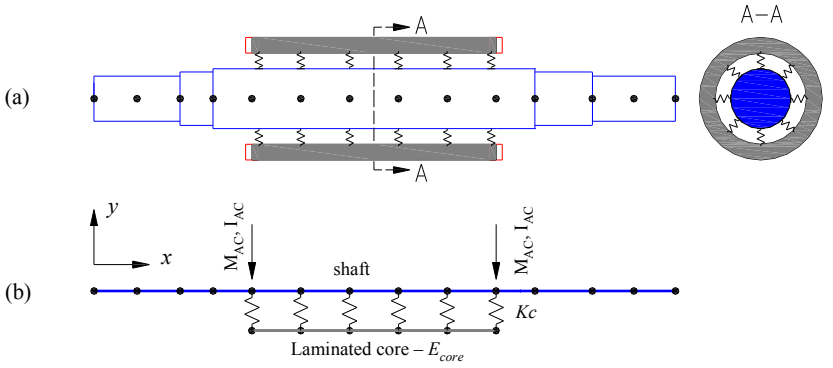

Fig. 3. Dual Rotor Arrangement for the Branched Model.

2.4. Numerical implementation

The three models described above were implemented using the commercial finite element software ANSYS rev. 11.0. A macro was developed in APDL (Ansys Parametric Design Language, see [8]) to build a parametric model for easy post-processing analysis. The basic data used for the rotor were the lengths of the shaft steps; the outer and inner diameter of each shaft step; the Young's modulus, Poisson's ratio and density for the shaft material; and the total mass of the lamination core. Three finite element types were used to represent the system: class C^1 Timoshenko's beam elements ([9]) for the shaft and laminated core in models 02 and 03; point mass elements (with mass and inertia moments) to

represent the discs in model 01; and one-dimensional spring elements to represent the interface between the shaft and the laminated core in model 03.

The discrete system for a rotordynamic analysis, written in matrix form, is given by ([3])

$$[\mathbf{M}]\ \{\ddot{\mathbf{q}}(t)\}+([\mathbf{C}]+[\mathbf{G}])\{\dot{\mathbf{q}}(t)\}+[\mathbf{K}]\ \{\mathbf{q}(t)\}=\{\mathbf{f}(t)\} \tag{5}$$

where $[\mathbf{M}]$ is the inertia or mass matrix, $[\mathbf{K}]$ is the stiffness matrix, $[\mathbf{C}]$ is the damping matrix, $[\mathbf{G}]$ is the gyroscopic matrix, $\{\mathbf{q}(t)\}$ is the nodal displacement vector, $\{\dot{\mathbf{q}}(t)\}$ is the nodal velocity vector, $\{\ddot{\mathbf{q}}(t)\}$ is the nodal acceleration vector and $\{\mathbf{f}(t)\}$ is the generalized force vector. However, as in this work the parameters are identified based on the natural frequencies of the system when it is stationary and the damping effect is neglected, Eq. (5) can be simplified to the following generalized eigenvalue problem [10]

$$[\mathbf{K}][\mathbf{\Phi}]=[\boldsymbol{\lambda}][\mathbf{M}][\mathbf{\Phi}] \tag{6}$$

where $[\boldsymbol{\lambda}]$ is a diagonal matrix containing the eigenvalues, each eigenvalue λ_i being related to ω_i, the *i*-th natural frequency, as follows: $\lambda_i = \omega_i^2$; and $[\mathbf{\Phi}]$ is a matrix in which each column contains the i-*th* eigenvector or natural mode associated with eigenvalue λ_i. Equation (6) is numerically solved using the Block-Lanczos method [11].

3. Experimental Modal Analysis

The experiments carried out in this study are intended to allow the modal parameters (natural frequencies and mode shapes) of squirrel cage rotors with different geometries to be obtained. The results were used to assess the performance of the three equivalent beam models implemented.

3.1. Rotors tested

No prototypes were developed specifically for the tests. Instead, the tests were performed using commercially available rotors manufactured by the Brazilian electric motor manufacturer WEG, with no control of the interference between the rotor core and the shaft. Table 1 gives a brief description of some of the features of the rotors tested. These were selected to include the commonest types of squirrel-cage rotors used in electrical machines.

Table 2 gives some of the geometric ratios of the rotors tested: the ratio between the length of the core and the length of the shaft (L_{CH}/L_{SHAFT}) , between the diameter of the plates in the core and the diameter of the shaft in the core region (ϕ_{CH}/ϕ_E), between the diameter of the yoke of the rotor plate and the diameter of the shaft in the core region (ϕ_{CO}/ϕ_E), between the height of the yoke of the rotor plate and the radius of the shaft in the core region (H_{CO}/R_E), between the total mass of the core and the mass of the shaft (M_T/M_{SHAFT}), between the length of the core and the diameter of the plates in the core (L_{CH}/ϕ_{CH}), and between the length of the core and the diameter of the yoke of the plates in the core (L_{CH}/ϕ_{CO}).

Table 1. Some Characteristics of the Rotors Tested.

Rotor identification (*)	Mass (kg)	Rotor characteristics
225IIP	70.0	Rotors with continuous aluminium bars, without ventilation channels (continuous core)
250IVP	141.0	
355IIP(A)	355.0	
355IIP(B)	367.0	
355IIP(C)	378.0	
315IIP	389.0	Rotors with aluminium bars and axial ventilation channels (continuous core)
400IIP	828.0	Rotors with copper bars and axial ventilation channels (continuous core)
450IVP	1224.0	
560IIP	1890.0	Rotors with copper bars and axial and radial ventilation channels (spaced cores)

(*) The first three figures are associated with rotor size. The next two figures, in Roman numerals, are associated with the number of poles and speed of rotation (for example, IIP corresponds to a rotor speed of 3600rpm, and IVP to a rotor speed of 1800rpm)

Table 2. Some Geometric Ratios of the Rotors Tested.

Rotor identification	$\frac{L_{CH}}{L_{SHAFT}}$	$\frac{\phi_{CH}}{\phi_E}$	$\frac{\phi_{CO}}{\phi_E}$	$\frac{H_{CO}}{R_E}$	$\frac{M_T}{M_{SHAFT}}$	$\frac{L_{CH}}{\phi_{CH}}$	$\frac{L_{CH}}{\phi_{CO}}$
225IIP	0.24	2.58	1.56	0.56	1.32	0.86	2.82
250IVP	0.37	3.05	2.20	1.20	3.01	1.27	3.78
355IIP(A)	0.33	3.18	2.03	1.03	2.97	1.29	3.75
355IIP(B)	0.33	2.87	1.83	0.83	2.52	1.29	3.95
355IIP(C)	0.33	2.41	1.54	0.54	1.76	1.29	4.39
315IIP	0.31	2.21	1.68	0.68	1.42	0.00	6.17
400IIP	0.28	1.80	1.40	0.40	0.87	1.65	7.44
450IVP	0.31	2.07	1.67	0.67	1.21	1.87	7.25
560IIP	0.31	2.04	1.57	0.57	1.20	2.12	8.33

3.2. Description of the experiments

All the rotors were tested in a free-free condition. Figure 4 shows the 560IIP rotor, which weighs approximately 2 tons, suspended by slings and a hoist. Data acquisition was performed using a Brüel & Kjær Type 3560C PULSETM four-channel data acquisition unit. Excitation was provided with the aid of ENDEVCO modal hammers: model 2203-5 for the 225IIP and 250IVP rotors, and model 8208 for the remaining ones[1]. The vibration peak was measured with a model 752A12 TEDS accelerometer, also from ENDEVCO.

[1] The type of the hammer used is directly related to the mass of the rotor being tested. Above a certain mass, the 8208 hammer had to be used, as this is suitable for heavy structures.

Fig. 4. Rotor Suspended for an Experimental Test in a Free-Free Support Condition.

The rotors were discretized as shown in Fig. 5 for the 560IIP rotor. Excitation was provided using a modal hammer at a point at the front of the shaft, Fig. 6, while an accelerometer scanned the other points on the rotor to measure the response. This ensures that the first vibration modes are obtained sequentially because there will never be a node at the extremities of the beam (the rotor) for the boundary conditions tested. Pulse Labshop software, which provides graphs of FRF (frequency response function) and coherence, was used for the data acquisition, and ME'scopeVES was used for the modal analysis. In all the measurements, ten averages were used for the FRF with a resolution of 1Hz. On average, the frequency range used extended from 10 Hz to 5 kHz. The signals were obtained using a uniform window for the hammer force and an exponential window for the response from the accelerometer.

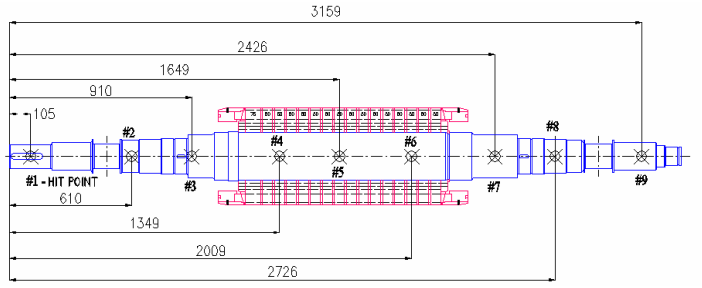

Fig. 5. Positions of the Excitation and Response Points (Distances in mm).

Fig. 6. Excitation and Measurement on the 250IVP Rotor.

3.3. Extraction of the modal parameters

The inertance curves were obtained from the modal analysis using techniques based on the theory described by Ewins [10]. The modal parameters were extracted in the frequency domain, using all the inertance curves of all the degrees of freedom (discrete measurement points) simultaneously. The minimum least squares method was used to estimate the modal parameters [12]. Table 3 shows a summary of the natural frequencies obtained experimentally for each rotor. The number of frequencies and corresponding vibration modes obtained for each rotor were defined by the frequency band in which the excitation of the modal hammer could be kept relatively constant (deviation less than 3 dB). For this reason, four modes could be obtained for some rotors, while for others only three were obtained. Although the modal damping was obtained experimentally, it was neglected in the numerical models.

Table 3. Natural Frequencies Obtained Experimentally (in Hz).

Rotor	Freq. #1	Freq. #2	Freq. #3	Freq. #4
225IIP	688	1203	2597	3039
250IVP	612	928	2169	2794
355IIP(A)	329	579	1290	-
355IIP(B)	395	683	1362	-
355IIP(C)	468	822	1384	-
315IIP	332	493	853	1140
400IIP	288	454	711	-
450IVP	167	302	527	710
560IIP	137	202	429	566

4. Comparison of Experimental and Numerical Results

4.1. Discrepancies between numerical and experimental results

The proposed beam models were evaluated by varying their parameters within a pre-established range. The first natural frequencies with their corresponding modes of vibration were then calculated. These frequencies and modes were compared with the modes obtained experimentally to determine the percentage error in the natural frequency calculated for each value of the parameter for a particular model in relation to the corresponding experimental values. This was done for each of the rotors and each beam model, and the error was plotted on a graph in each case, as shown in Figs. 7, 8 and 9 for the 225IIP rotor. The lines marked with lozenges, squares, crosses and triangles correspond to the variation (absolute value) in the error of each first natural frequency, while the solid red line represents the average error as a function of the parameter used in each model.

Figure 10 shows a comparison of the vibration modes obtained experimentally and numerically using the three models in the minimum error condition for the 355IIP(A) rotor. It can be seen that all the modes obtained numerically match those obtained experimentally.

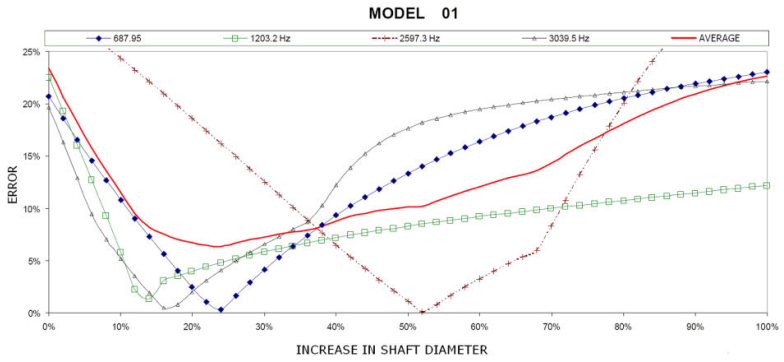

Fig. 7. Error in the Natural Frequencies for the 225IIP Rotor – Model 01.

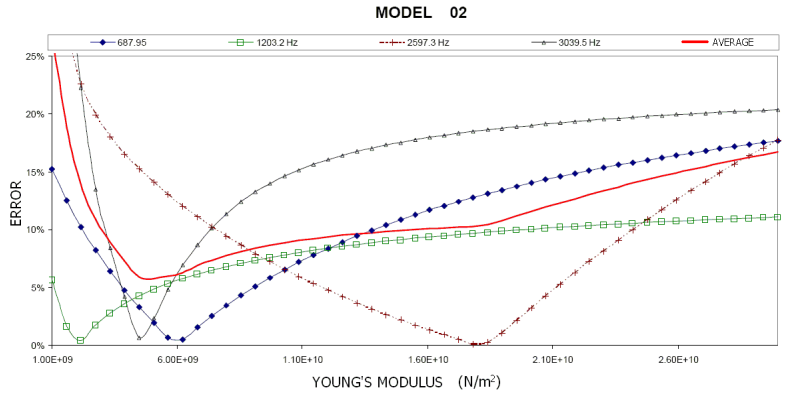

Fig. 8. Error in the Natural Frequencies for the 225IIP Rotor – Model 02.

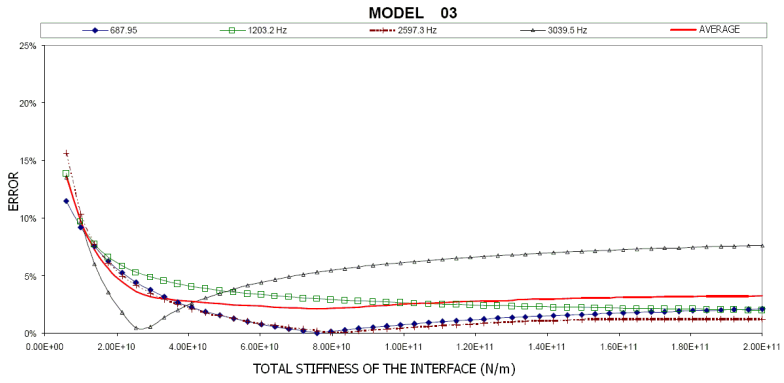

Fig. 9. Error in the Natural Frequencies for the 225IIP Rotor – Model 03.

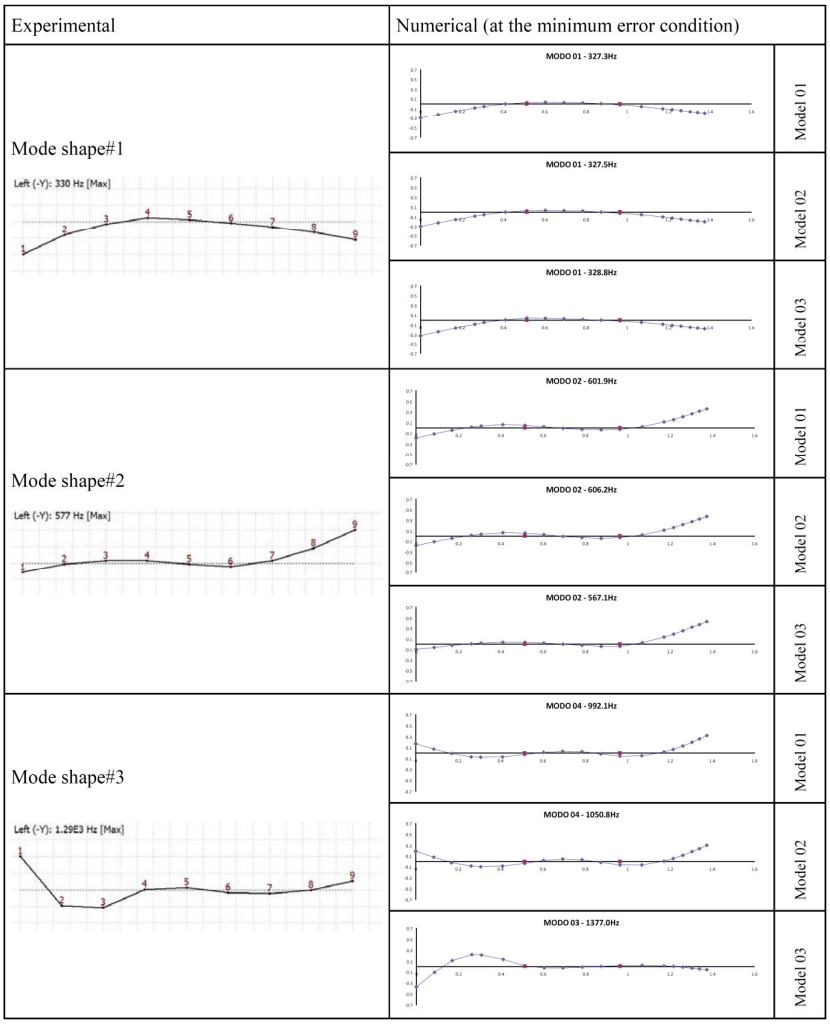

Fig. 10. Comparison of the Mode Shapes for the 355IIP(A) Rotor.

4.2. Evaluation of the accuracy of the models

It can be seen that there are many points in the graphs in Figs. 7, 8 and 9 that minimize the numerical error and exactly fit the natural frequencies for each rotor mode shape but correspond to different parameter values. This indicates that the stiffness effect changes for each mode when equivalent beam models are used to represent rotors with laminated cores. In an ideal model, one would be able to use a single parameter value to reproduce all the dynamic characteristics of a rotor. Therefore, to evaluate how close to ideal the equivalent beam models are, the following criterion is proposed: *the less dispersed the parameter values that minimize the error in each mode shape, the more accurate will be the equivalent model for a given rotor*.

Based on the graphs above (and the corresponding graphs for the other rotors), we can use the average error curve to obtain information about the accuracy of the model. The accuracy of the equivalent model will therefore be determined by the value of the minimum average error, which is henceforth referred to as minimum error. Accordingly, the smaller the minimum error, the more accurate is the model. Table 4 shows the minimum error values obtained for each model for each rotor tested and the number of modes considered for each rotor. According to these results, model 03 is the most accurate for almost all the rotors tested (six of the nine). Additionally, we can infer that models 01 and 02 can be considered equal in terms of accuracy. This conclusion was reported by Garvey et al. [7], who state that the branched model is quite appropriate for representing rotors with laminated cores.

Table 4. Minimum Error in the Natural Frequencies for Each Equivalent Beam Model.

Rotor	Model 01	Model 02	Model 03	No. of modes
225IIP	6.4%	5.8%	2.1%	04
250IVP	12.5%	10.2%	6.0%	04
355IIP(A)	9.2%	8.5%	1.9%	03
355IIP(B)	6.8%	6.1%	1.8%	03
355IIP(C)	2.7%	2.6%	1.2%	03
315IIP	3.1%	2.3%	3.7%	04
400IIP	1.9%	1.7%	0.3%	03
450IVP	3.0%	2.1%	4.4%	04
560IIP	3.6%	3.2%	4.0%	04

Since the final objective is to determine whether the same beam model can be used to represent various rotor geometries without having to identify the parameters for each case experimentally, the information on accuracy is incomplete. The model must also be sufficiently robust for its characteristics not to change substantially as the input parameters are changed when different types of rotors are being modeled. The following section therefore describes the second criterion used in this paper to evaluate the equivalent beam models.

4.3. Evaluation of the robustness of the models

The following robustness criterion was used in this work: *using a single parameter value for the equivalent beam model, is the model still capable of calculating the first natural frequencies of all rotors accurately?*

Table 5 shows the parameter values corresponding to the minimum error condition shown in Table 4 for each model and rotor. The average of these parameter values for all the rotors for a particular model is then used as a fixed value to recalculate the natural frequencies. The new average error values for the N first natural frequencies are shown in Table 6. It can be seen that for model 03 the average error remains below 5% in almost all the rotors tested (six of the nine) using only one value for the parameter for this model. The exceptions were the 250IVP and 450IVP rotors.

Table 5. Parameter Values at the Minimum Error.

Rotor	Model 01 *pt (%)*	Model 02 E_{core} (GPa)	Model 03 *Kc* (N/m)
225IIP	23.9%	5.1	7.6×10^{10}
250IVP	55.2%	14.0	9.9×10^{09}
355IIP(A)	42.4%	6.2	5.6×10^{10}
355IIP(B)	45.6%	9.7	1.7×10^{11}
355IIP(C)	29.6%	10.0	4.9×10^{10}
315IIP	30.0%	17.0	3.3×10^{10}
400IIP	15.6%	16.0	1.8×10^{10}
450IVP	10.0%	6.2	1.1×10^{10}
560IIP	28.8%	21.0	4.1×10^{10}
Average	31.2%	12.0	5.1×10^{10}

Table 6. Average Error in the Natural Frequencies for the *N* First Natural Frequencies with a Fixed Parameter.

Rotor	Model 01	Model 02	Model 03
225IIP	7.4%	9.3%	2.4%
250IVP	20.1%	11.5%	9.7%
355IIP(A)	15.%	10.6%	2.1%
355IIP(B)	13.5%	6.7%	2.8%
355IIP(C)	3.2%	3.3%	1.3%
315IIP	3.3%	4.5%	4.0%
400IIP	6.7%	2.5%	3.4%
450IVP	16.1%	5.8%	13.3%
560IIP	3.8%	5.7%	4.2%

5. Concluding Remarks

In this work, three beam models for representing the dynamic influence of the laminated core of electrical machine rotors were implemented and evaluated. The models were evaluated by comparing the natural frequencies and mode shapes obtained numerically and experimentally. Nine different squirrel-cage rotors were used for the experiments. Two methods for evaluating the models were described. In the first, a curve of mean error for all modes was plotted against the variable parameter for each model. The minimum value of this curve was used to define the accuracy of the beam model in question for each of the rotors tested. On average, model 03 (the "branched model") proved to be the most accurate in reproducing the natural frequencies of the nine rotors tested. The second evaluation method was based on the criterion of model robustness, i.e., whether a single parameter value could be used in the model to represent all the rotors tested. In the first method for evaluating the models, the value of the parameter at minimum error for a particular model varied between rotors. The mean of these

parameter values for all the rotors was then used as a new fixed evaluation parameter to recalculate the average error in the *N* first natural frequencies of a given rotor. Model 03 proved to be the most robust in the majority of cases but had a large error for two of the rotors analysed. Apart from these two exceptions, this model had a mean error of less than 5% using a single parameter value.

Acknowledgement

The authors would like to thank the Brazilian funding agency FINEP under the project PROMOVE 4931/06 and WEG Company for the financial support.

References

1. Ehrich, F.F. (2004). *Handbook of rotordynamics* (3nd Ed.). Florida: Krieger Publishing Company.
2. Lalanne, M.; and Ferraris, G. (1990). *Rotordynamics prediction in engineering* (1st ed.). England, John Wiley & Sons Ltd.
3. Wowk, V. (1994). *Machinery vibration: Balancing*. McGraw Hill, Inc., USA.
4. API 684 - *American Petroleum Institute Standards* (2005). API Recommended Practice 684: Rotordynamics tutorial - lateral critical speeds, unbalance response, stability, train torsionals, and rotor balancing. Washington, D.C.
5. Kim, Y.C.; and Kim, K.W. (2006). Influence of lamination pressure upon the stiffness of laminated rotor. *JSME International Journal*, 49(2), 426-431.
6. Chen, Y.S.; Cheng, Y. D.; Liao, J. J.; and Chiou, C.C. (2008). Development of a finite element solution module for the analysis of the dynamic behavior and balancing effects of an induction motor system. *Finite Elements in Analysis and Design*, 44(8), 483-492.
7. Garvey, S.D.; Penny, J.E.T.; Friswell, M.I.; and Lees, A.W. (2004). The stiffening effect of laminated rotor cores on flexible-rotor electrical machines. In: *IMECHE - International Conference on Vibrations in Rotating Machinery*, Swansea, UK, 193-202.
8. ANSYS User's Manual, Version 11.0 (2008). *Swanson Analysis Systems Inc.* (SASI), Houston, PA.
9. Genta, G. (2005). *Dynamics of rotating systems* (1st Ed.). New York: Springer.
10. Ewins, D.J. (1984). *Modal testing: Theory and practice* (1st Ed.). Great Britain: Research Studies Press Ltd.
11. Bathe, K.J. (1996). *Finite element procedures* (1st Ed.). New Jersey: Prentice Hall.
12. ME'scopeVES Version 4.0.0.6 (2003). *Operating Manual: Volume II - Reference*. Vibrant Technology, Inc.